Airborne RFI Measurements with PSR/CXI and CISR in the Chesapeake Bay Region: Initial Data Examination

November 8, 2004

Contents

1 Introduction **2**

2 Instrumentation **2**
- 2.1 PSR/CXI 2
- 2.2 CISR 4
- 2.3 Interface Between PSR/CXI and CISR 5
- 2.4 Measurement Process 6

3 Experiment Conditions **7**

4 Pax River to Wallops Flight **10**
- 4.1 Spectrometer Channel Results 12
- 4.2 CISR Spectra Results 14

5 Low Altitude Pass over DelMarVa **19**

6 Portion of Hex-Cross Lines over Buoy **25**

7 Stare Mode During Transit back to WFF **31**

8 Summary and Discussion **38**

1 Introduction

This report provides initial documentation of observations of C-band RFI made from the US Navy's P-3 research aircraft using the PSR/CXI system of NOAA/ETL and the C-band Interference Suppressing Radiometer (CISR) digital backend of the Ohio State University (OSU) ElectroScience Laboratory. The observations described in this report were performed during a test flight on Oct. 8th, 2004 prior to departure of the aircraft for the AMSR-E Antarctic Sea Ice (AASI) cal-val campaign on Oct. 9th. Only data for which both CISR and PSR/CXI information was available are discussed here, in particular only the horizontally polarized C-band measurements. The PSR/CXI instrument also recorded vertically polarized channels, but these were not sampled by CISR during the flight.

2 Instrumentation

2.1 PSR/CXI

Reference [1] provides a description of the combined PSR/CXI and CISR system; here the relevant information is briefly reviewed. The PSR/CX instrument of NOAA/ETL has been deployed in several previous airborne remote sensing campaigns [2], and provides well calibrated brightness measurements along with a variety of possible scanning patterns during flight operations. The majority of the data to be presented were obtained from conically scanned observations (i.e. the antenna is rotated in azimuth at a fixed speed) at a fixed incidence angle of 55 degrees from nadir (when in level flight). One set of observations in "stare" mode is also presented; in this case, the antenna is maintained at a fixed, forward-looking azimuth angle, again at a fixed incidence angle of 55 degrees. The antenna 3 dB beamwidth is approximately 8 degrees for all observations.

The PSR/CX instrument includes four C-band sub-channels, at frequencies of 5.8-6.2, 6.3-6.7, 6.75-7.1, and 7.15-7.5 GHz. These sub-channels can provide some measure of RFI mitigation, but remain large analog channels ($\sim$400 MHz bandwidth) compared to the bandwidth of likely RFI sources. The PSR/CXI instrument utilized

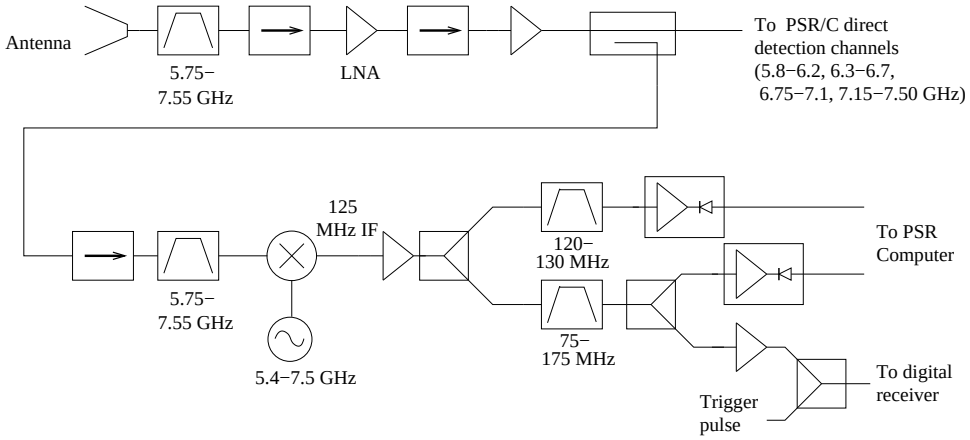

Figure 1: Simplified schematic of PSR/CXI

in this flight is a modification of PSR/CX that includes a downconverter module so that tuned observations can be made throughout C-band in a narrower bandwidth than the 400 MHz of the main channels. Figure 1 is a simplified schematic of the PSR/CXI, and shows that following initial filtering and front-end amplification, a portion of the antenna power is coupled to the downconverter section. The local oscillator (LO) utilized is capable of tuning from 5.4 to 7.5 GHz, uses a 125 MHz IF center frequency, and provides > 20 dB rejection of the upper RF side band. The IF signal is filtered to both 10 and 100 MHz bandwidths, and both of these bandwidths are passed through a logarithmic amplifier/detector, power integrated, and recorded. The 100 MHz bandwidth signal is also passed through a linear amplifier; a portion of this coherent signal is coupled to the CISR instrument in the cabin rack of the P-3, while the remainder is detected, power integrated, and recorded by PSR/CXI (PSR/CXI post-amplifier section not shown in Figure 1).

For the data reported here, the LO was tuned so that 100 MHz channel observations were made at 5.5-5.6, 5.6-5.7, ..., 7.6-7.7 GHz; this is a set of 22 channels. The LO was swept continuously throughout the flight, with each channel being observed for approximately 38 msec; a complete sweep of channels required approximately 836 msec. The PSR/CXI LO is a YiG-tuned device [3], and therefore is subject to hysteresis effects as well as temperature sensitivity. For this reason, the accuracy of the RFI frequencies should be taken as $\approx \pm 2$ MHz throughout this report. Although this

is acceptable accuracy for radiometric studies, it is recommended that an LO with improved tuning accuracy and stability be considered for future flights of PSR/CXI.

2.2 CISR

A simplified schematic of the CISR instrument is provided in Figure 2. The CISR digital receiver backend measures the incoming 100 MHz bandwidth through the use of two 200 MSPS A/D converters, each of which samples the band 125-175 MHz. A "channel-selection" is therefore required to upconvert the 75-125 MHz portion of the PSR/CXI IF signal to 125-175 MHz. Following A/D conversion, the CISR instrument can perform an "asynchronous pulse-blanking" (APB) [4] operation to suppress temporally localized interference, as well as a 1024 point FFT operation, followed by optional power integration or max-hold computations. The following digital receiver modes were utilized in the Oct. 8th test flight:

- Mode 0: Integration, APB off
- Mode 1: Integration, APB on
- Mode 2: Max-Hold, APB off
- Mode 3: Max-Hold, APB on
- Mode 4: Capture

In Modes 0 to 4, the 1024 point FFT operation is performed, followed by power computation and the integration or max-hold operations. The output in these modes is then a spectrum of the power in 1024 $\sim$100 kHz bandwidth sub-channels within the tuned 100 MHz spectrometer channel. This finer spectral resolution can provide improved capabilities for identifying and suppressing frequency-localized interference. The final "capture" mode refers to direct recording of the sampled 100 MHz channel at 10 nsec temporal resolution with no further processing.

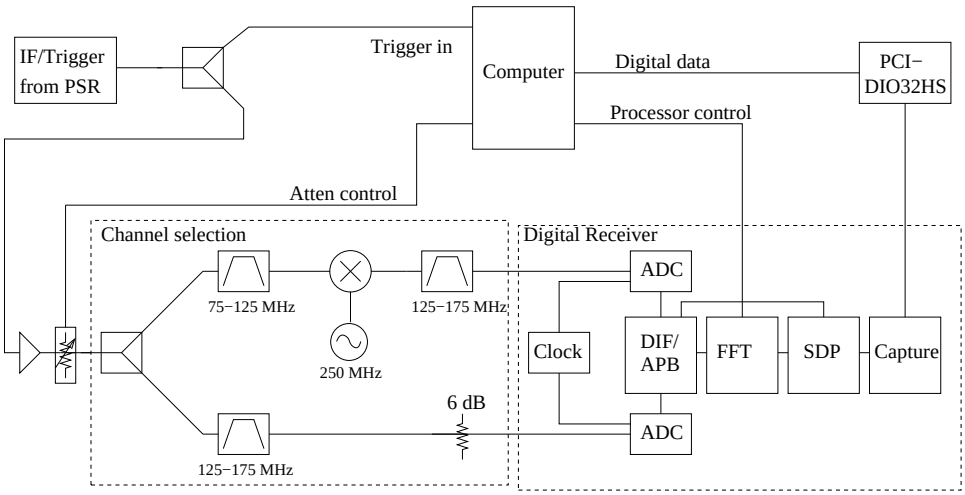

Figure 2: Simplified schematic of CISR

2.3 Interface Between PSR/CXI and CISR

Because it is the PSR/CXI data acquisition computer that controls oscillator tuning in the downconverter, the CISR and PSR/CXI computers must be interfaced. To make this interface as simple as possible, a simple 1-bit "trigger" signal was used. This TTL-level pulse is sent from the PSR/CXI control computer to the CISR computer whenever a tuning operation has been completed and measurements should begin. In addition, both computers include highly accurate on-board clocks, synchronized through the IRIG-B standard, so that knowledge of the oscillator frequency for a particular CISR measurement is obtainable by matching up recorded trigger pulse times in post-processing of a joint data set. In the data considered here, unambiguous matchups of the PSR/CXI and CISR measurements were possible utilizing this process. Offsets in the two "timestamps" were within 5 msec for the majority of the recorded data.

One issue in this time synchronization involves observations of the internal noise diodes of the PSR/CXI system. These noise diodes are useful for verifying system stability between measurements of the external hot and cold targets embedded in the PSR/CXI scanhead. The simple 1-bit trigger interface however does not allow specification of the noise diode switch state during a measurement. To address this issue, a plan was developed wherein the noise diode measurements were to be performed

within a specified time interval following the trigger signal. However, the time accuracy of the PSR/CXI instrument states was insufficient to ensure an accurate noise diode measurement by CISR at each opportunity. For example, although the mean time delay between trigger pulses was 38 msec as planned, and 86% of delays were within 37 to 39 msec, in some cases time delays between triggers as short as 24.5 and as long as 140 msec were observed. It is recommended that future work address this issue by providing more precise control of PSR/CXI instrument state timing. Initial analysis of PSR/CXI measured noise diode data also shows some evidence of scene and/or RFI corruption, possibly caused by these timing issues as well.

2.4 Measurement Process

As stated previously, the PSR/CXI LO was continuously tuned through the 22 bands of interest throughout flight operations, requiring approximately 836 msec to complete a sweep. When in conical scan mode, the PSR/CXI antenna rotation period was typically 2.9 seconds, so that 3.45 sweeps were performed per antenna "scan" (i.e. rotation). The resulting combined spatial and spectral sweeping process makes interpretation of the tuned data somewhat difficult, as will be discussed in subsequent sections.

The CISR mode (i.e. "average, APB off", etc.) was switched every 4 sweeps, or slightly more than every rotation of the antenna. In CISR modes 0 to 4, a base temporal resolution of 1.3 msec was utilized, with 12 1024 point spectra (either integrated or max-held) obtained in 15.75 msec following each PSR/CXI trigger. In the capture mode, a 128K capture (1.3 msec) was recorded for each PSR/CXI trigger. CISR required approximately 2 seconds to record measured data to the on-board harddrives following a sweep of modes 0 to 4. The resulting CISR data rate is approximately 10 GB/hr; although this is certainly unacceptable for end-user radiometer applications, the goal of recording as much information on the observed RFI as possible results in the high data rate for this study. CISR includes 120 GB of on-board storage, and two 300 GB external hard drives are available for archiving of flight data through a USB 2.0 interface to the CISR computer.

The PSR main channel data to be reported was "quick-calibrated" using the external hot and cold loads of the PSR scan head; this procedure is expected to produce brightnesses typically accurate to within 1-2 K. The PSR "VIEWRAD" processing system was utilized for this purpose, as well as for forming scan images of measured brightnesses. A calibration procedure for the tuned PSR/CXI and CISR channels has not yet been developed. Relative variations of the raw data from these channels are examined, and provide useful information on observed RFI properties. The possibility of corruption of the PSR main channel calibration procedure due to strong RFI during external cal-target observations should be noted; the joint data set will be examined in future work for any evidence of such problems.

3 Experiment Conditions

Table one provides information on the test flight plan. Figure 3 illustrates the geographical region observed; note the Patuxent River Air Station (PAX), Wallops Flight Facility (WFF), and NDBC buoy 44009 are marked with blue, red, and black circles respectively. As can be seen in Table 1, the flight plan included an initial transit from PAX to WFF from 13:34 to 13:51 UTC, followed by several low altitude lines over the DelMarVa peninsula for RFI studies after takeoff from WFF at 16:13 UTC, followed by observations over NDBC buoy 44009 in a hex-cross pattern, then return to WFF at 18:01. A final flight section returned from WFF to PAX, landing at 18:46. The stopovers at WFF were required in this test flight to support calibration and testing operations for the ATM and D2P laser instruments that were also on-board the aircraft.

Both the PSR/CXI and CISR instruments successfully recorded data on the initial PAX to WFF flight (approximately 10 minutes of joint data), on a portion of the flight lines over DelMarVa and transit to the hex-cross pattern (approximately 24 minutes of joint data), and throughout the entire hex-cross pattern and transit back to WFF (57 minutes). These observations were all in conical scan mode, with the exception of the cal-roll measurements and the stare mode observations from 17:52 to 18:01 on return to WFF from the buoy pattern. The CISR instrument data was not recorded

Time (UTC)	Event	Comments
13:34	Takeoff from PAX	Short transit flight PAX to WFF
13:39	Start data collection	
13:49	Stop data collection	
13:51	Land at WFF	
16:13	Takeoff from WFF	Low altitude lines over DelMarVa
16:17	Start data collection	CISR off
16:40	Continue data collection	CISR on
16:54	Exit lines over DelMarVa	Start transit to buoy 44009
17:04	Begin hex-cross pattern over buoy	
17:42	End hex-cross pattern over buoy	Prepare for cal-rolls
17:45	Begin set of 3 60 degree cal rolls	
17:52	Finish cal rolls	Begin transit to WFF, stare mode
18:01	Land at WFF	
18:28	Takeoff from WFF	
18:32	Begin data collection, stare mode	No PSR data
18:44	End data collection	No PSR data
18:46	Land at PAX	

Table 1: Time history of test flight on Oct. 8th, 2004

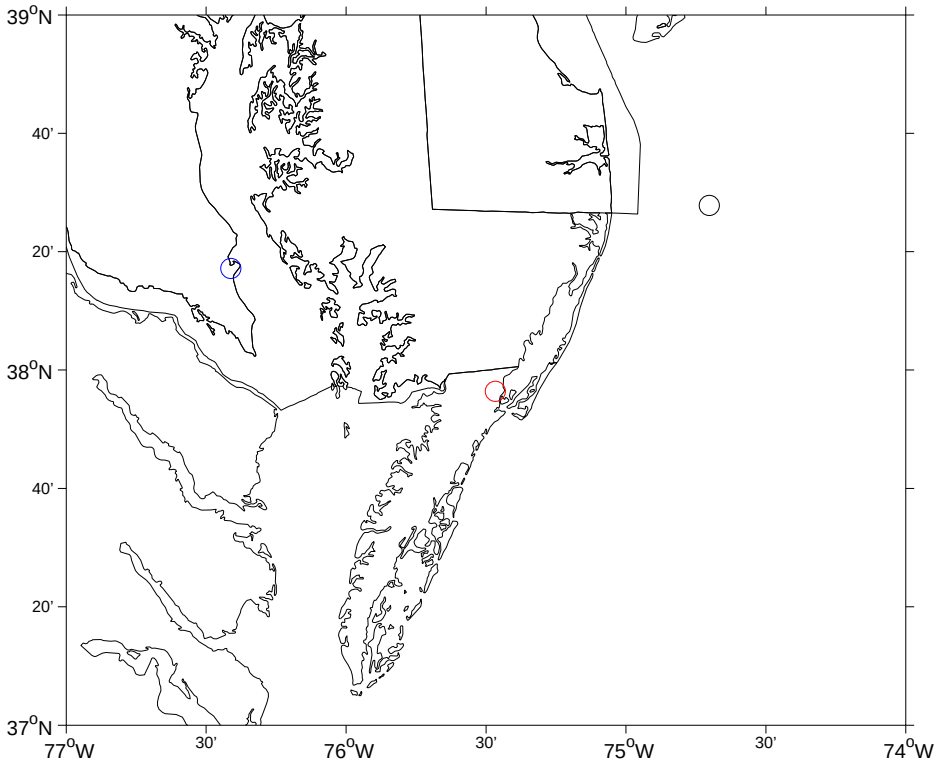

Figure 3: Regional map of test flight area, including Patuxent River Air Station (blue circle), Wallops Flight Facility (red circle), and NDBC buoy 44009 (black circle)

for the initial DelMarVA observations, while the PSR/CXI data was not recorded during the final transit back to PAX. Overall the observed data set still contains a variety of useful scenes for RFI investigations, including both land and near-coastal regions.

At present, the detailed navigational data for the flight is not available. However the basic flight plan discussed combined with the land/water scenes observed make basic interpretation of these data possible. Detailed geo-location of the measured data will be performed once the full navigational data is obtained. The images to be illustrated formed from PSR/CXI conically scanned data will be presented in terms of time and scan angle; these should not be taken as geographic images given possible variations in the aircraft heading, pitch, roll, and altitude.

The following sections present and discuss subsets of the measured data for the major sections of the flight plan, including the initial transit flight from PAX to WFF, a portion of the low-altitude lines over DelMarVa, a portion of the hex-cross pattern over the buoy, and a portion of the stare-mode data on the return to WFF.

4 Pax River to Wallops Flight

Figure 4 illustrates PSR/CXI scan images for the four main channels (5.8-6.2, 6.3-6.7, 6.75-7.1, and 7.15-7.5 GHz, labeled channels 1 to 4 respectively) during the initial PAX to WFF transit flight. The color scale is calibrated brightness temperature in Kelvins, and the backward looking portion of the scan is shown. It should be expected that the flight altitude as well as direction is varying rapidly throughout this short flight, so a direct correlation of the scan image to a geographical image should not be expected. However the image clearly contains both land and water observations, with strong RFI evident due to the large differences among channels in some image portions. The largest RFI contributions are up to 1410K in channel 3 around time 13:47. Although strong RFI is not obvious in the channel 4 image, the possibility of weak RFI remains.

In order to examine data from the 22 tuned PSR spectrometer and CISR channels, the effects of LO tuning must be considered. It should be noted that the possibility

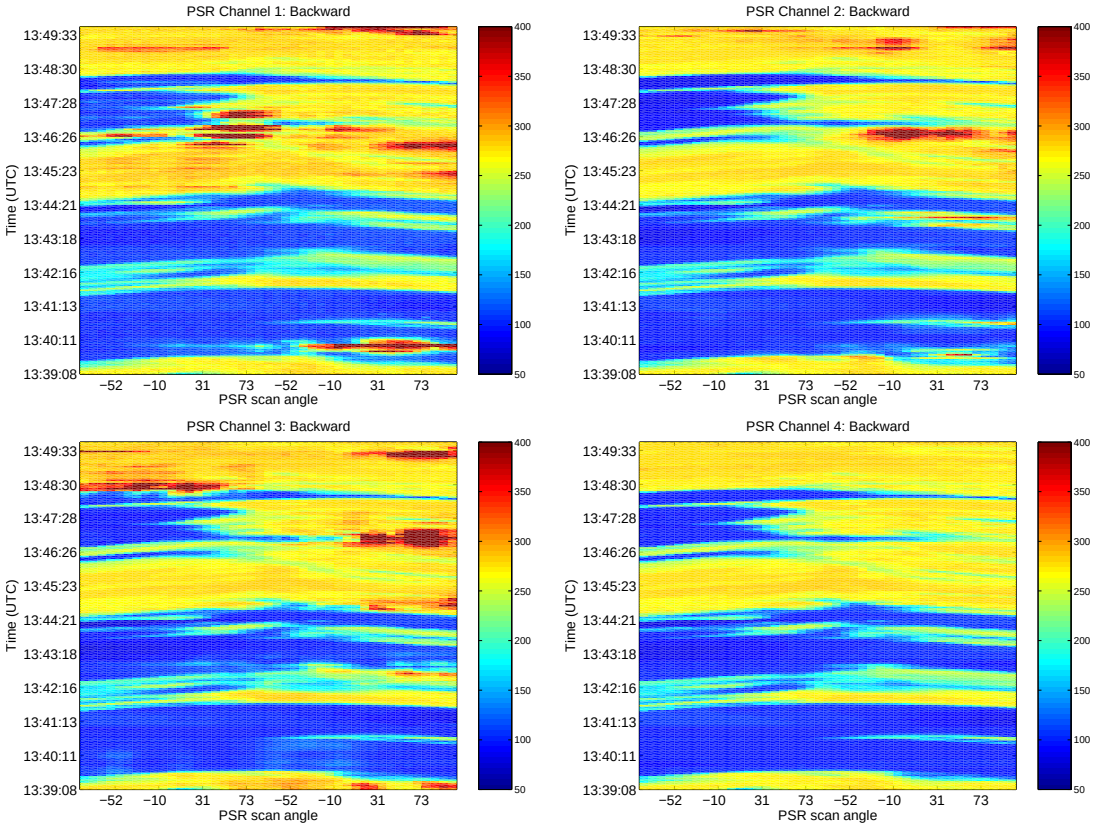

Figure 4: Calibrated brightnesses observed in 4 PSR main channels for backward looking portion of PAX to WFF transit flight

exists for the tuned channels to fail to observe RFI recorded by the PSR main channels, because the spectrometer was not tuned to the RFI frequency when the source was in the antenna pattern. Also, it is not possible to form scan images similar to those of Figure 4 for these channels, because each image pixel is recorded at a different center frequency in the tuning process. While it is possible to examine the time history of a specific spectrometer channel, successive measurements of a given channel can be time separated by as much as 836 msec, again making correlation of a channel time history to the PSR main channel scan images difficult.

To address this issue, an interactive data analysis tool (IDAT) was developed. The IDAT tool overlays symbols on the main channel scan images that indicate the spectrometer channel observed in a particular image pixel. It is then possible for the user to select a pixel and examine the particular PSR spectrometer channel and CISR measurements corresponding to that pixel. The connection between the main channel scan images and spectrometer channel time histories is thus established through this tool.

Although IDAT makes it possible to examine possible sources of RFI observed in the PSR main channel images, it is not possible to demonstrate use of this tool in a hard-copy report. For this reason, spectrometer and CISR data will be illustrated through time history plots, with IDAT results reported in the discussion.

4.1 Spectrometer Channel Results

Figure 5 illustrates time histories for the 10 MHz PSR logarithmic channel, the 100 MHz PSR logarithmic channel, the 100 MHz PSR linear channel, and the 100 MHz total power measured by CISR. Because these are raw data tuned over the instrument passband, normalization of the images is required to produce reasonable results. For the logarithmic channels, the data in each of the 22 channels was first transformed as if in decibels to a linear representation. The mean of this linear representation over time was then converted to decibels and subtracted from the data each channel. Of course, the measured data likely contains an offset with respect to the decibel power, so this is not a precise normalization of the receiver noise power; improved

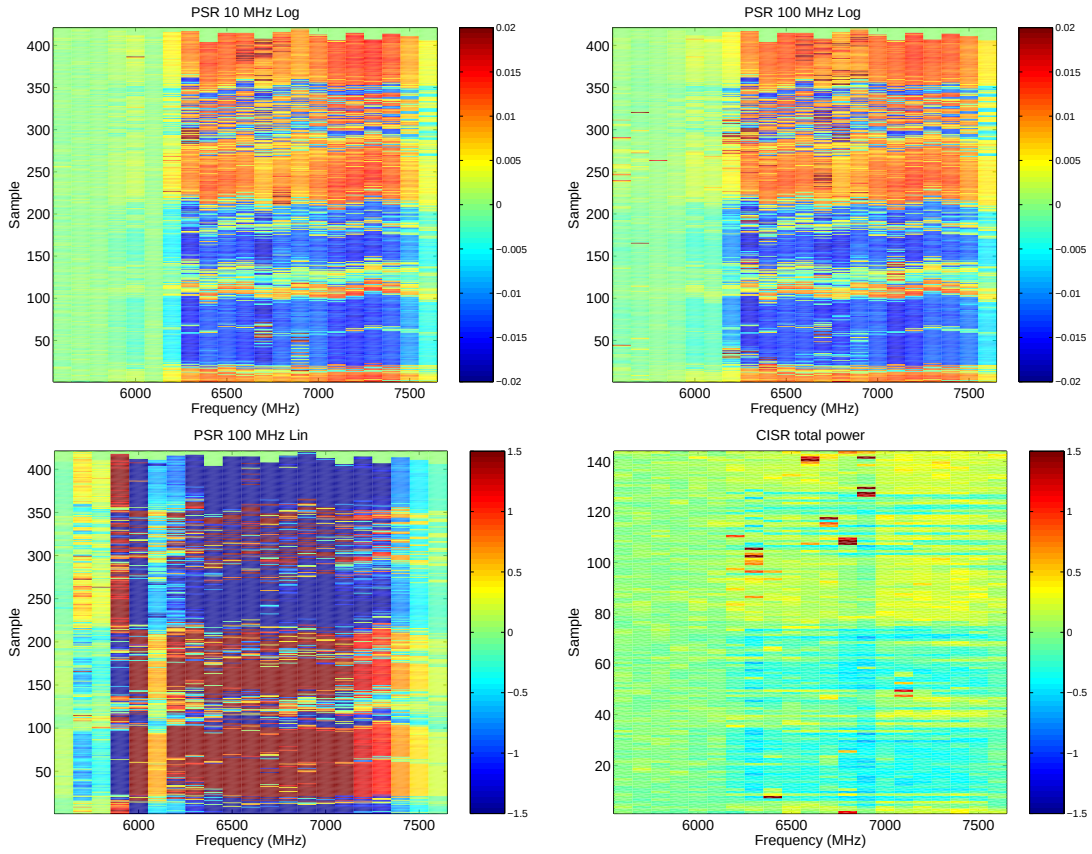

Figure 5: Time histories of the PSR 10 MHz log, PSR 100 MHz log, PSR 100 MHz linear, and CISR total power measurements, in 22 channels. See text for a description of the normalizations utilized and color scales.

methods will be considered in the future. For the PSR linear and CISR total power figures, the data in each channel was divided by its average over time, and the result converted to decibels. It should be noted that the mean computations in both cases can be severely biased high in channels containing strong RFI, making normalized results in the absence of RFI appear lower than nearby channels. Procedures will be considered in the future to eliminate this effect by computing the mean only over a smaller amplitude subset of the data.

The results in Figure 5 clearly capture the land/water variations in the scenes of Figure 4; note the 100 MHz linear spectrometer channel has a negative overall gain in some image portions that results in the mostly inverted image for this case. The log channels show a significantly reduced contrast in the channels below ~6.2 GHz; this is likely due to the lower front end gain for the lower channels and the absence of a

normalization relative to the standard deviation of each channel. All channels show some evidence of large amplitude samples, for example around 6.05 GHz, sample 375 in the 10 MHz log channel, 5.55 GHz, sample 240 in the 100 MHz log channel, and frequencies from 6.3 to 7.0 GHz, samples 80 to 140 in the CISR measurements.

4.2 CISR Spectra Results

Figures 6-8 illustrate time histories of 1024 point sub-channels from the CISR instrument for each of the 22 spectrometer channels. Only the Mode 0 results (average, APB off) are illustrated, and a normalization identical to that for the CISR total power measurements in Figure 5 is used in each of the 1024 sub-channels. The much higher spectral resolution obtained in these data allows a higher contrast image of observed RFI to be obtained, as well as the identification of high amplitude but narrowband RFI that is not easy to identify in total power results.

Results in Figure 6 for the first 8 spectrometer channels show some evidence of narrowband RFI at frequencies of 5572, 5595, 5605, 5812, 6018, 6212, and 6270 MHz; here narrowband refers to observed 3 dB bandwidths up to 3-4 MHz. IDAT analysis of other CISR modes also showed narrowband sources near 5633 and 6135 MHz. Wider band RFI with bandwidths up to 20 MHz is also observed near 6190 MHz and 6255 MHz. IDAT analysis shows that the 6190 MHz interferer is strongly correlated to the large amplitude RFI observed near UTC 13:39 in PSR main channel 1, as well as the strong RFI observed around UTC 13:45 and scan angles larger than 30 degrees. The strong 6255 MHz interferer also is significant in the latter case. The many narrowband sources do not produce extremely strong RFI in Figure 4, but when detailed analysis is performed it is possible to locate contributions on the order of 10-100 K from these sources.

Results in Figure 7 for spectrometer channels 9 to 16 again show the presence of both narrowband and wideband sources, with the latter occurring more frequently than in Figure 6. Narrowband sources near 6328, 6390, 6586, 6675, 6790, 6808, and 6827 MHz are observed, as well as wideband sources near 6370, 6555, 6615, 6675, 6685, 6735, 6755, 6765, 6810, 6835, 6855, and 7040 MHz. The strong RFI observed

in PSR main channel 2 (Figure 4) around time 13:46 is correlated to the interferers at 6255, 6328, and 6765 MHz, while the strong RFI observed around time 13:43 in the same image is correlated to the narrowband 6390 MHz source. The 6810 MHz source also produces strong RFI in the main channel 2 and channel 3 images around time 13:49. The wideband sources at 6685 and 6765 MHz are also strongly correlated to strong RFI in the PSR main channel 3 image in Figure 4 around 13:46, and the 6835 MHz source is related to the main channel 3 image around time 13:48, negative scan angles. The source at 7040 MHz also produces RFI in the main channel 3 image near times 13:42 for positive scan angles.

Results in Figure 8 show a lower level of apparent RFI in spectrometer channels 17 to 22 compared to the lower channels. Narrowband sources at 7228, 7478, and 7655 MHz are observable in IDAT analysis with CISR modes 1 to 4 however, and contribute to low level RFI in the PSR main channel 4 image. The latter two sources are observed primarily in portions of the main channel 4 image from times of 13:48 on.

Further studies will examine the extent to which RFI removal processing of the CISR data could potentially remove RFI contributions in the PSR main channels. In addition, the performance of the APB algorithm will be examined for these sources. Finally, the high resolution "capture" mode data of CISR will be examined to classify the detailed temporal and spectral properties of these interferers, so that effective RFI mitigation strategies can be designed. Note that in most cases of strong interference, the four-channel RFI removal algorithm used previously with the PSR main channels [2] would likely remove RFI contributions effectively, particularly for the scene of Figure 4 where main channel 4 apparently has little overall corruption. However lower level RFI from the narrowband sources observed by CISR would likely be more difficult for this algorithm to remove, making the potential gains of the CISR system more apparent in this case.

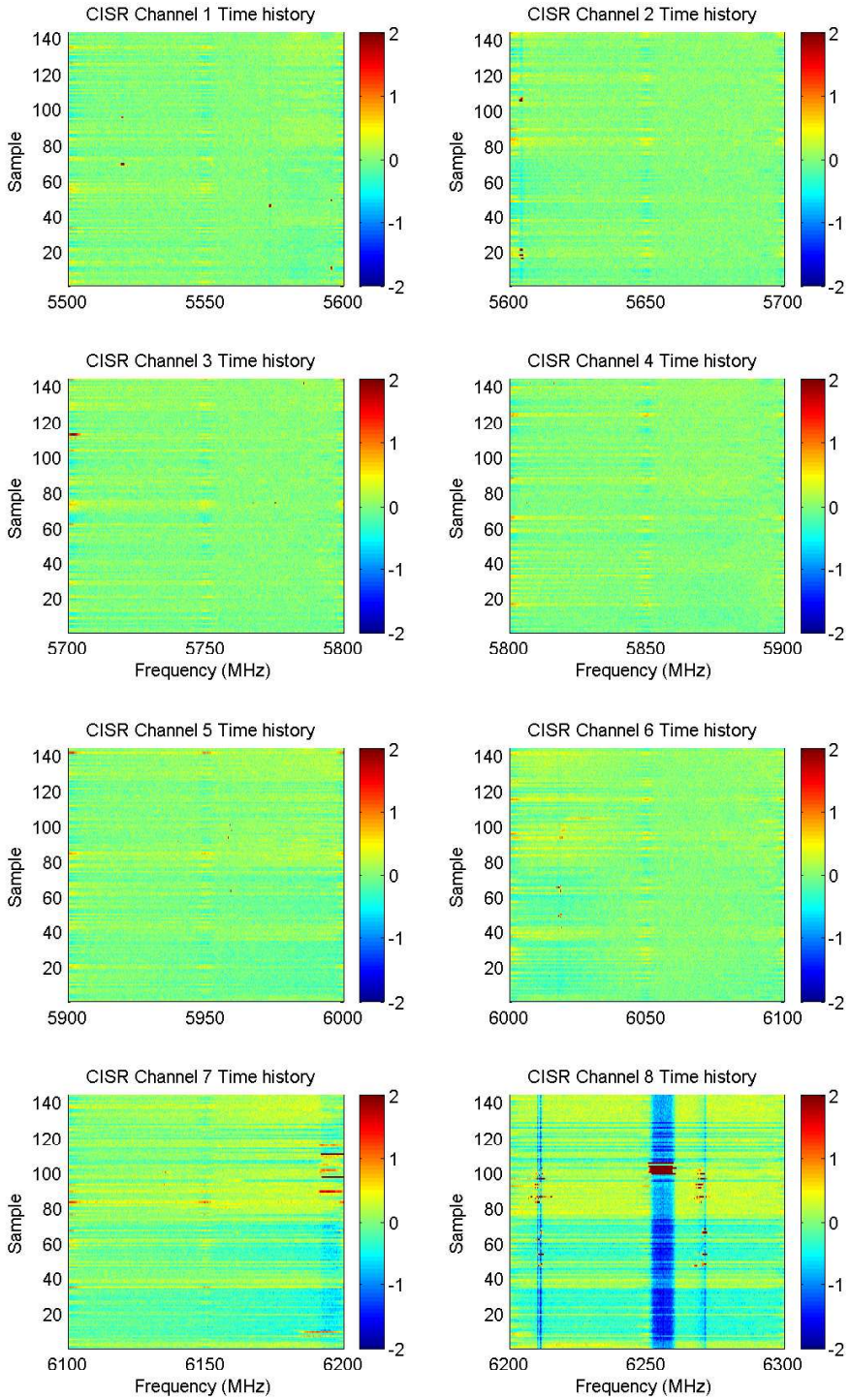

Figure 6: Time histories of CISR channels 1 through 8 in Mode 0. Color scale is in decibels.

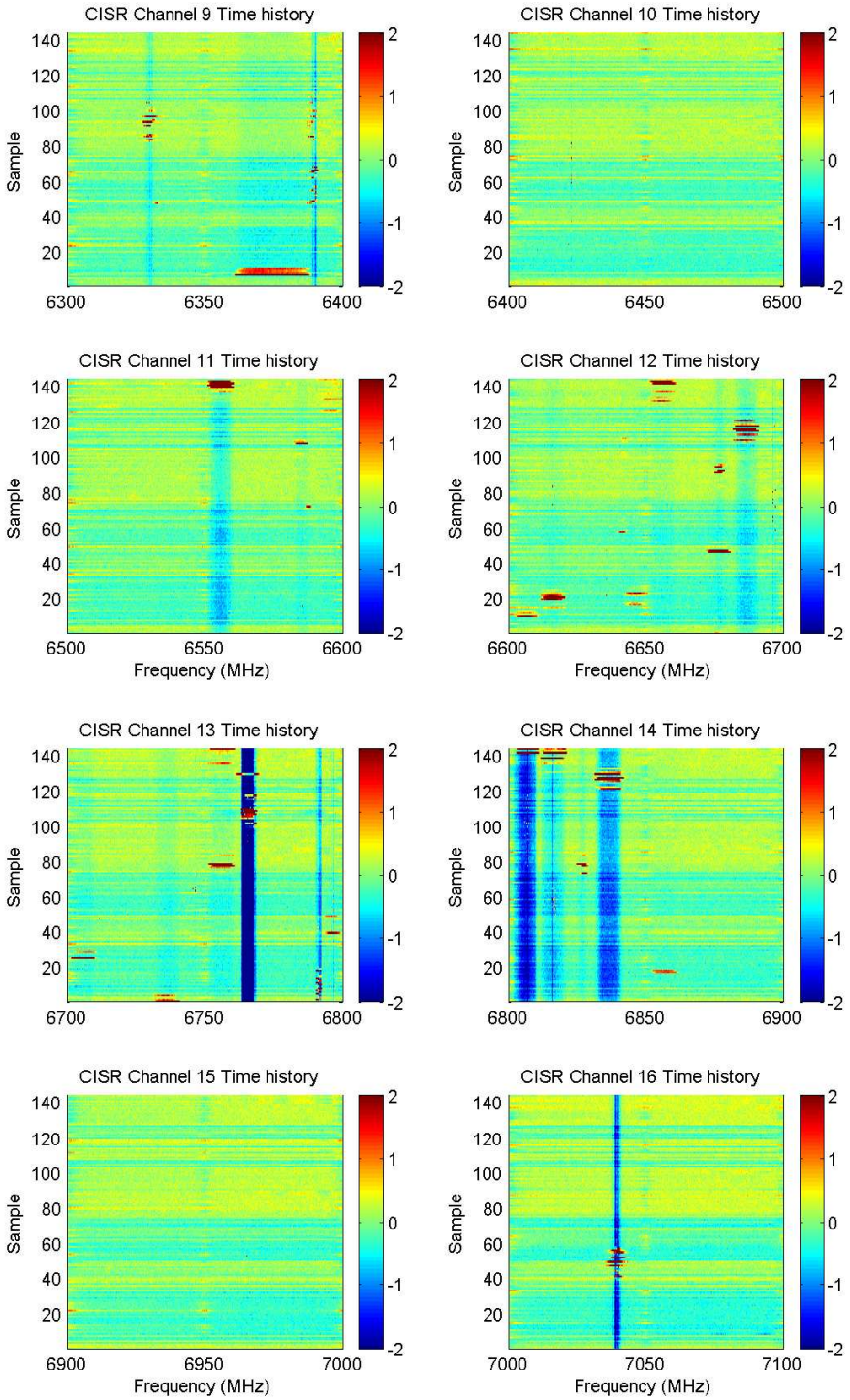

Figure 7: Time histories of CISR channels 9 through 16 in Mode 0. Color scale is in decibels

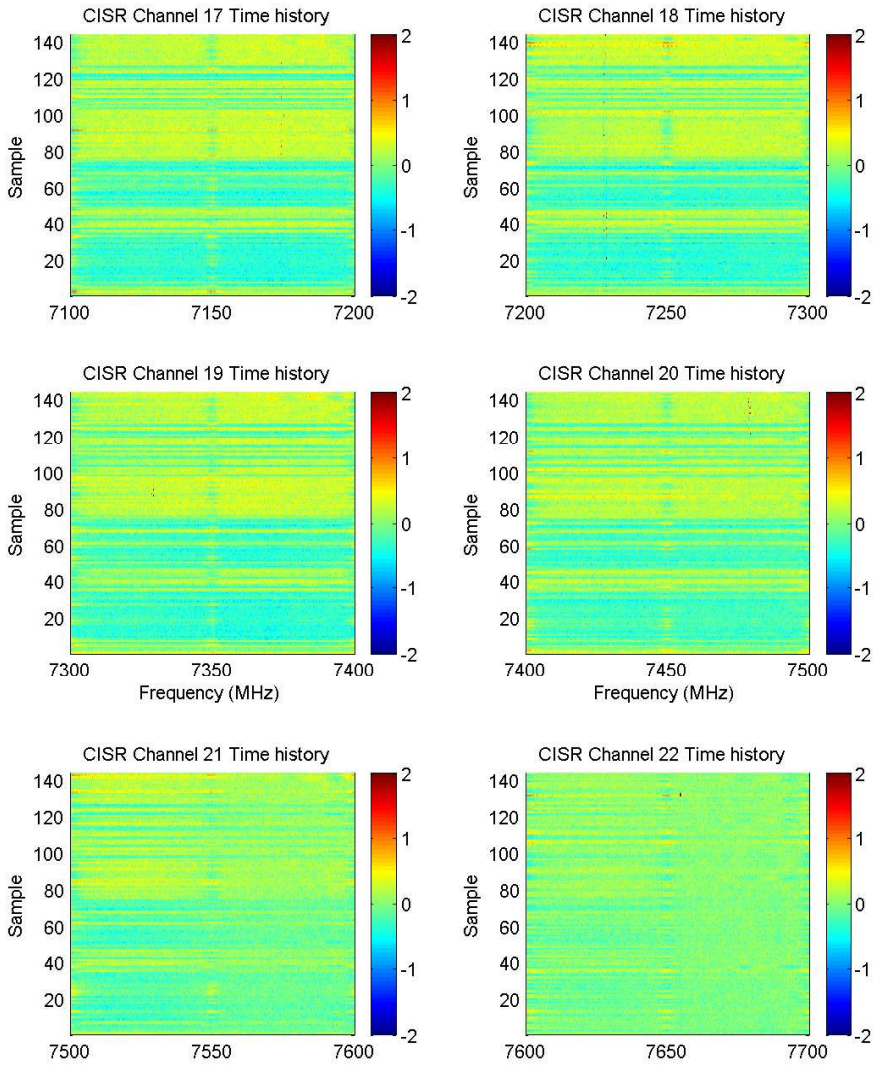

Figure 8: Time histories of CISR channels 17 through 22 in Mode 0. Color scale is in decibels

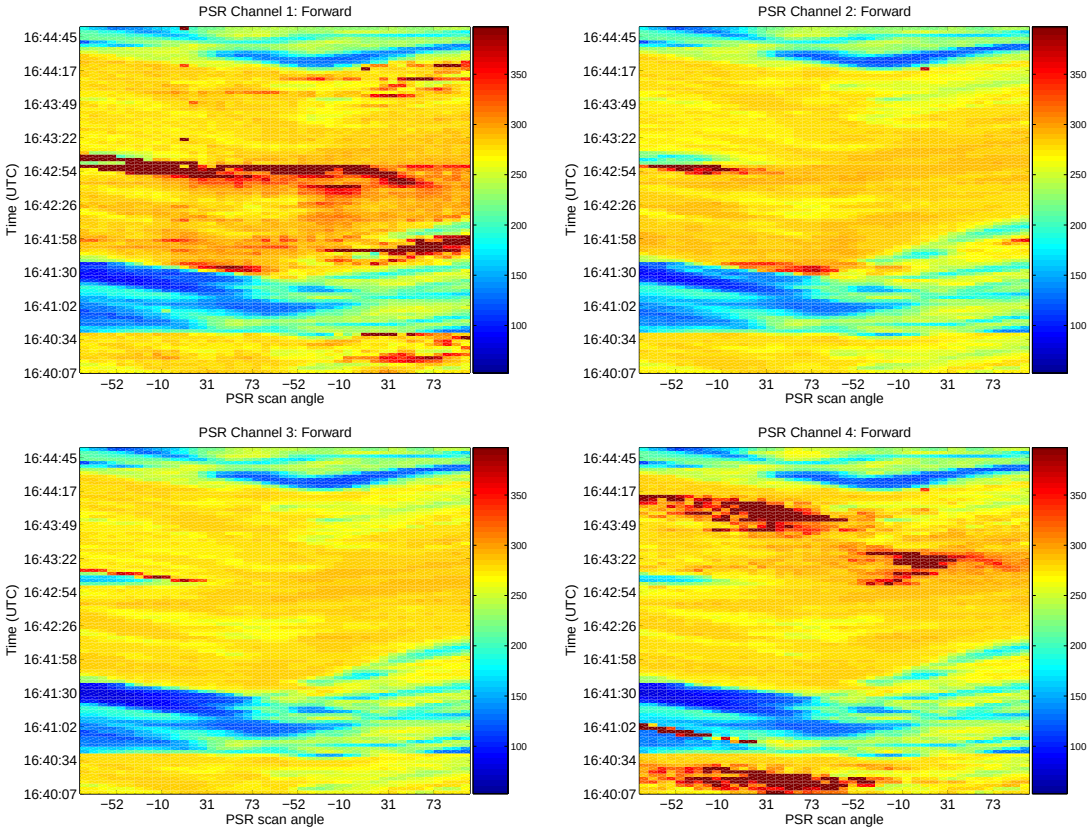

Figure 9: Calibrated brightnesses observed in 4 PSR main channels for forward looking portion of a low-altitude pass over DelMarVa peninsula

5 Low Altitude Pass over DelMarVa

Figure 9 illustrates calibrated brightnesses from the 4 PSR main channels during the forward looking portion of one low altitude pass over the DelMarVa peninsula. Again the presence of strong RFI (up to 5660K in channel 1 and 2843K in channel 4) is obvious in these images through a comparison of the four channels, and each of the four channels contains evidence of RFI at some location. In this case, channel 3 appears the least corrupted of the 3 channels, in contrast to Figure 4 where channel 4 had the least evidence of RFI.

Figure 10 again illustrates the time histories of the PSR spectrometer channels and the CISR total power. RFI is evident in all channels, with the 10 MHz channel capturing particularly strong samples at 6 and 6.7 GHz, while the remaining channels

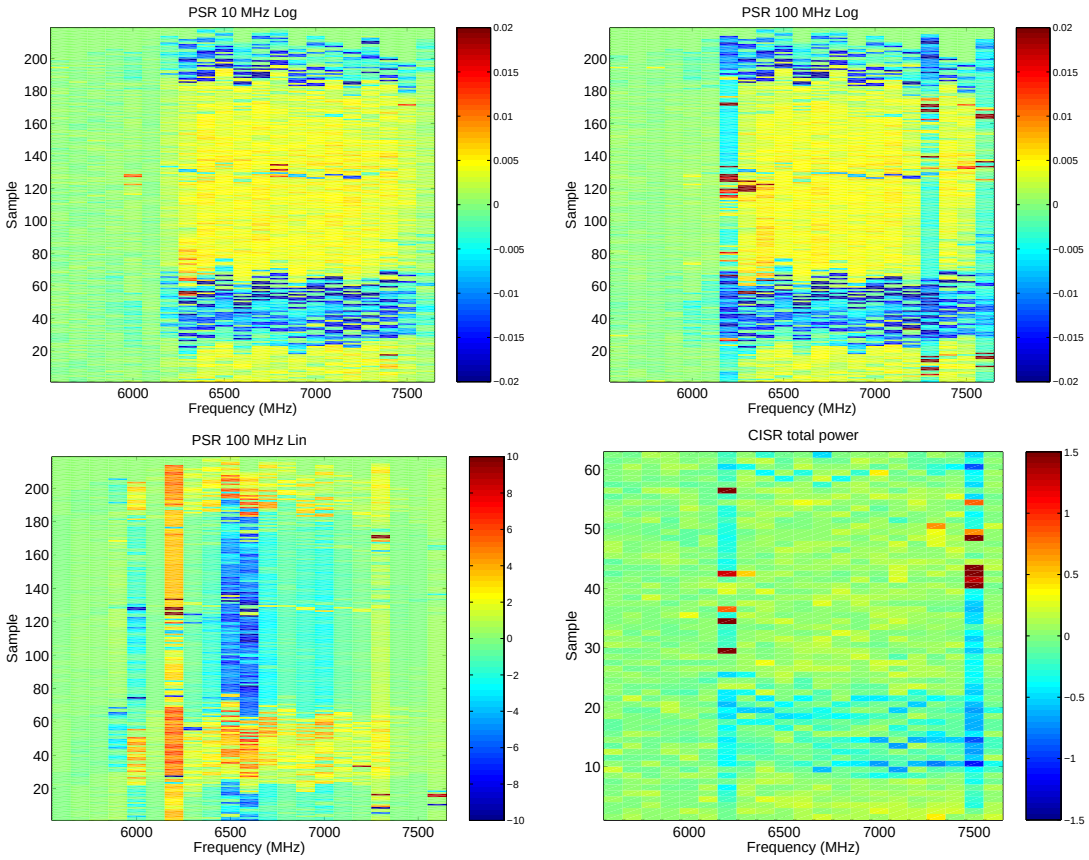

Figure 10: Same as Figure 5.

all show strong evidence of RFI in the 6.1-6.2 GHz band. The CISR total power channel also shows strong RFI evidence in the 7.4-7.5 GHz channel.

CISR spectra for spectrometer channels 1 to 8 in Figure 11 show a dominant wideband interferer at 6190 MHz (likely the same source as was observed in the transit flight), as well as narrowband interference at 5958, 6163, 6207, and 6265 MHz and other more intermittent sources. IDAT analysis shows the 6190 MHz source to be correlated to the strong RFI in PSR main channel 1 at times 16:40, 16:41:58, and 16:42:54. The source at 6163 MHz also appears in the RFI at 16:41:58, while the 5958 MHz source appears at time 16:42:54. The 5958 MHz source is also related to the large response observed in the 10 MHz PSR spectrometer channel. The sources at 6207 and 6265 MHz appear correlated to the PSR main channel 1 and 2 images around time 16:42:54 as well.

Figure 12 shows narrowband RFI at 6387 and 6740 MHz, among other smaller sources, and the IDAT analysis finds further wideband sources around 6755 and 6810 MHz (not observed in the CISR Mode 0 data). Again the dark lines observed at some frequencies are due to normalizations in these plots that include some large amplitude data outside the time range considered. The sources at 6387 and 6740 MHz appear correlated to the PSR main channel 2 RFI response around 16:41:30, while the 6755 and 6810 MHz sources are related to the response in channel 3 around time 16:42:54.

CISR spectra in channels 17 to 22 in Figure 13 are dominated by a wideband source at 7480 MHz and a smaller wideband source at 7600 MHz, while narrowband sources at 7171 and 7224 MHz are also observed. The wideband sources appear in the large amplitude portions of the PSR main channel 4 image around times 16:40, 16:41:02, and 16:43 to 16:44. The narrowband sources produce smaller observable contributions in both the PSR main channel 3 and 4 images, particularly in the water portion of the image at times 16:40 to 16:41.

A comparison of the results from the transit flight and the DelMarVa overpass clearly demonstrates that a variety of C-band sources can be observed, and that it is unlikely that any PSR main channel will be free of RFI throughout a sustained series of observations.

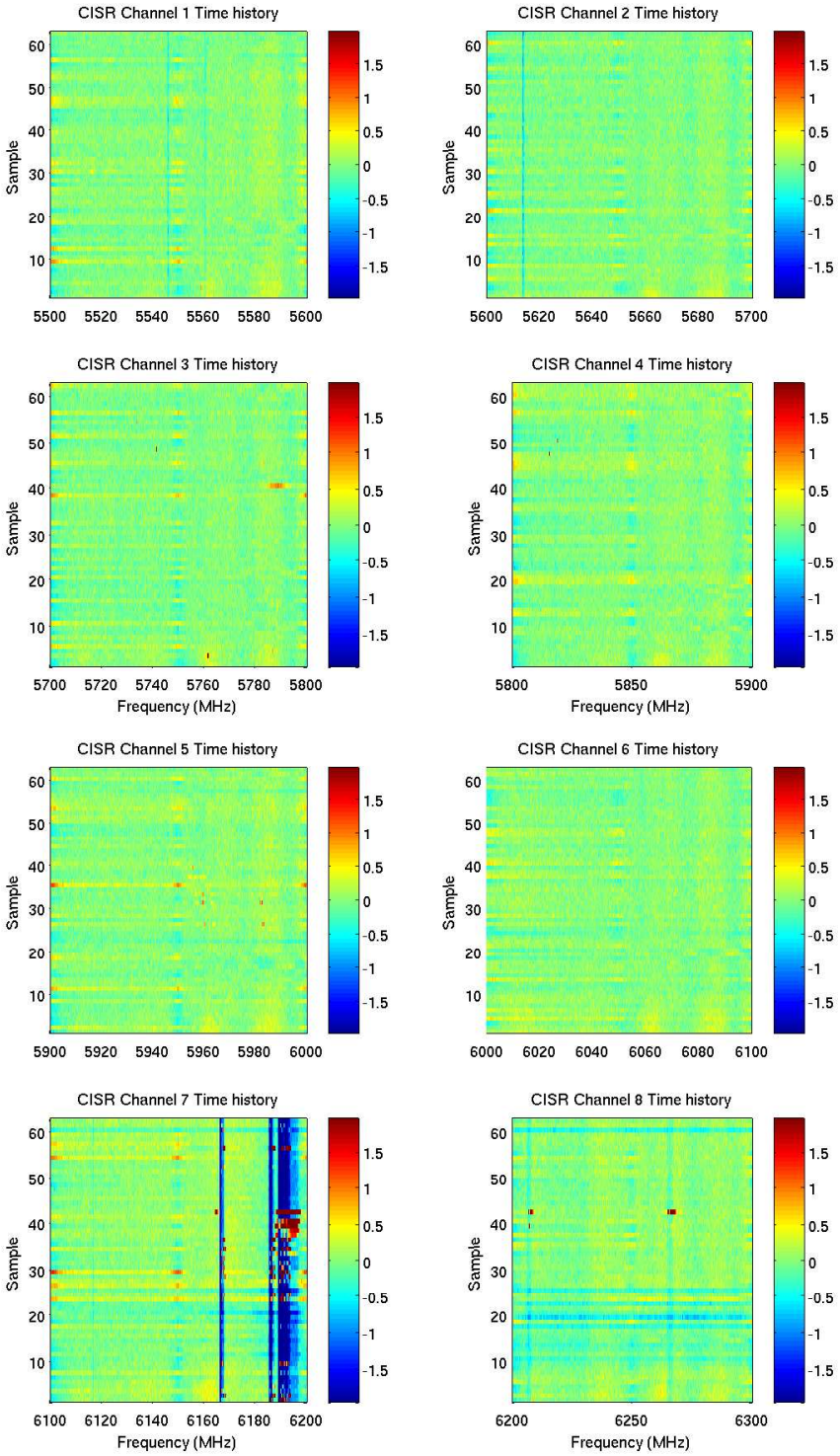

Figure 11: Same as Figure 6

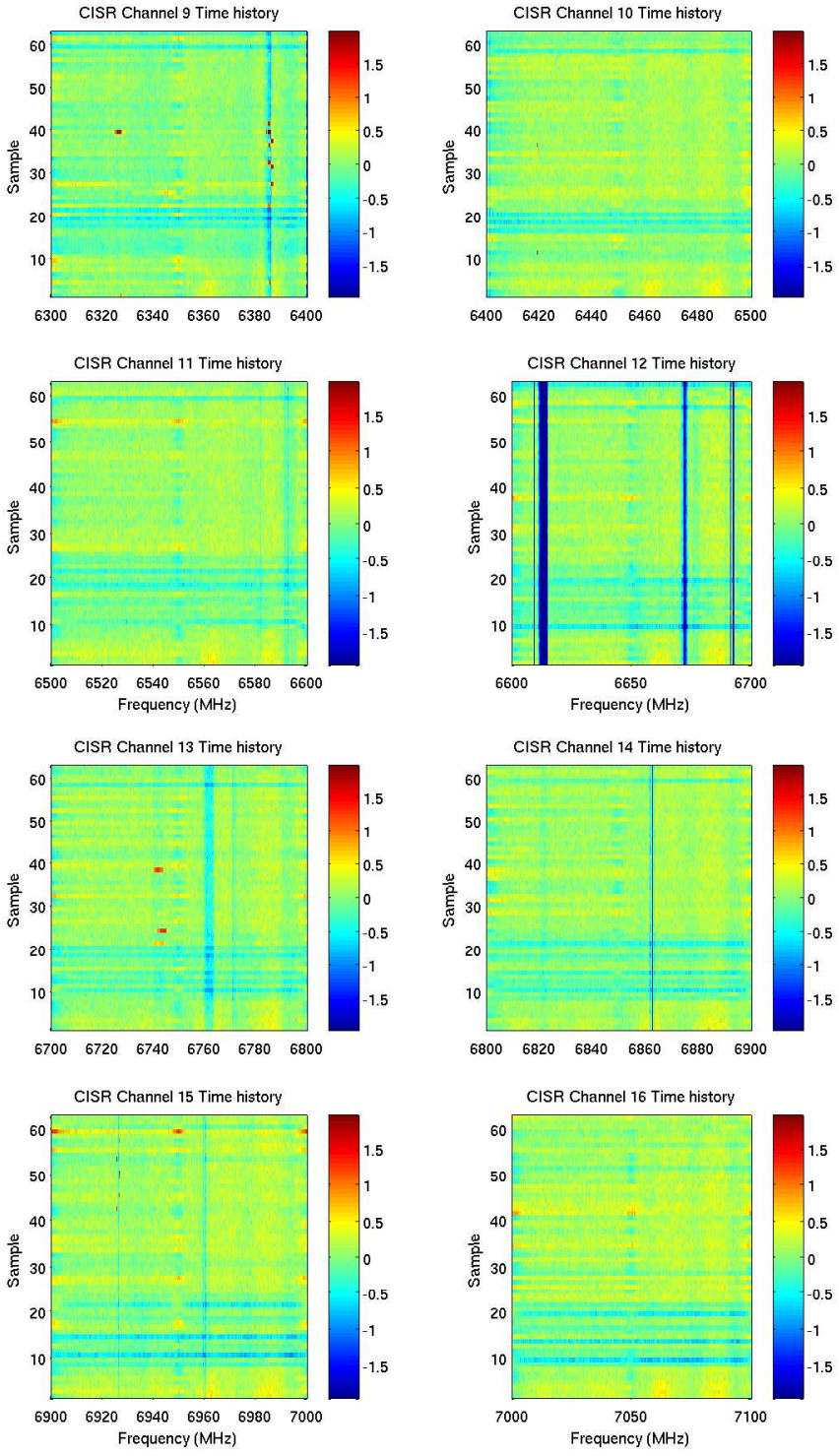

Figure 12: Same as Figure 7

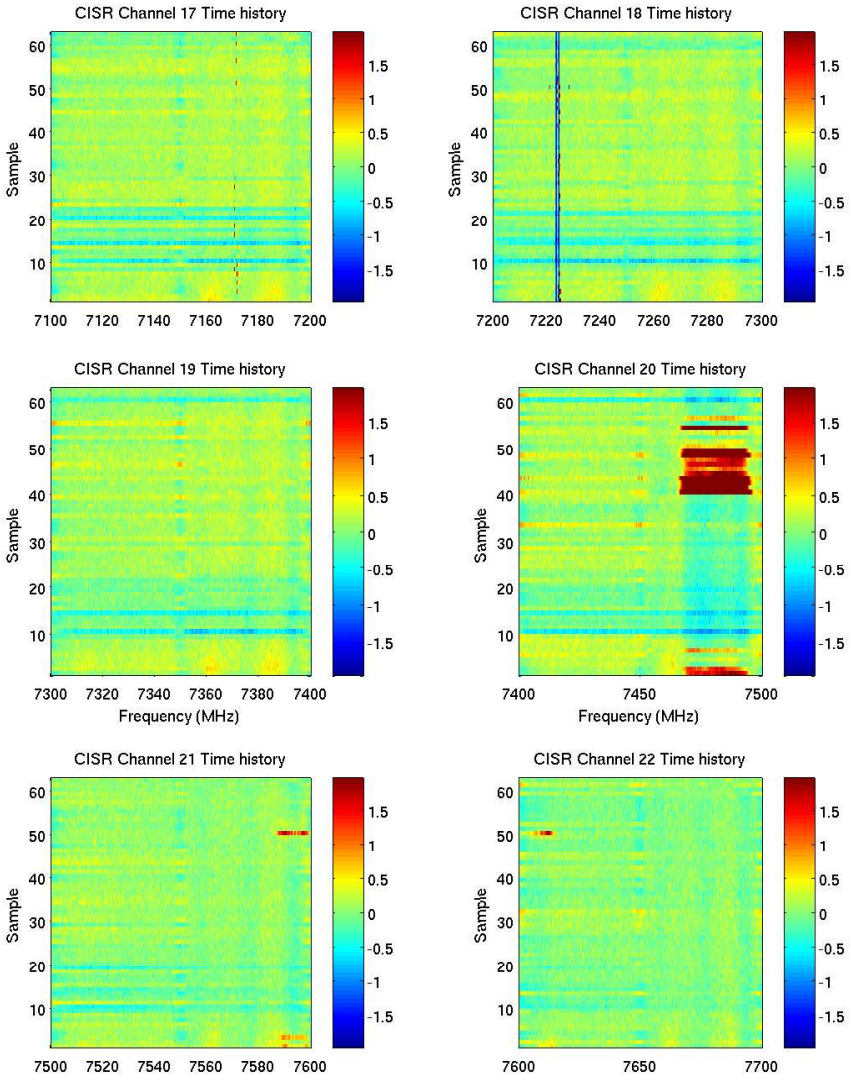

Figure 13: Same as Figure 8

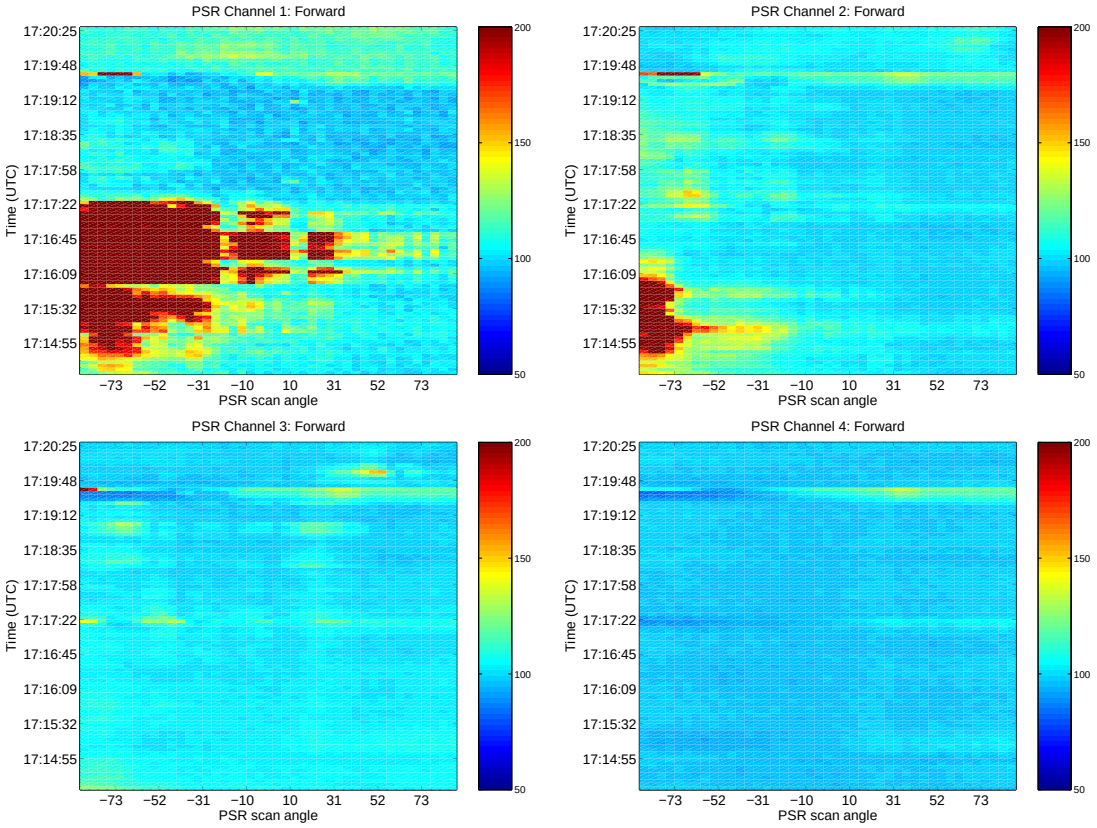

Figure 14: Calibrated brightnesses observed in 4 PSR main channels for forward looking portion of portion of hex-cross line over NDBC buoy 44009

6 Portion of Hex-Cross Lines over Buoy

Figure 14 illustrates PSR main channel brightnesses for a portion of the hex-cross overflight of NDBC 44009. This is "line two" of the hex-cross flight, and follows an eastward overflight of the buoy and turn to a S-SW heading. For this all sea scene, strong RFI (up to 3183K in channel 1, 1259K channel 2) is still observed. This is likely due to the presence of ships in these heavily used shipping lanes. A strong response is observed in all four PSR channels around time 17:19:40; the cause of this response is not known, and could possibly be a linearity or calibration problem for the PSR front end, possibly due to the strong RFI in channels 1 and 2 in a portion of the images at this time.

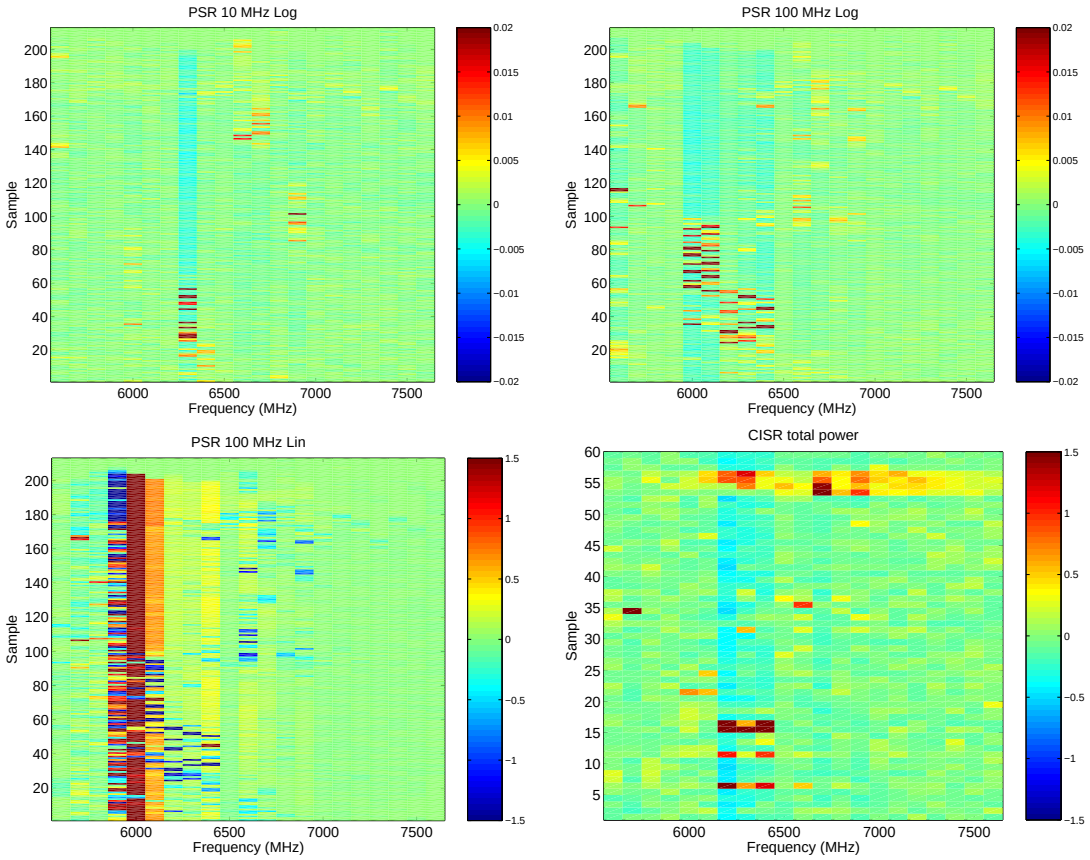

Figure 15: Same as Figure 5

The spectrometer channel plots in Figure 15 show RFI that is more easily detectable, due to the more homogeneous scene considered. All channels show evidence of RFI from approximately 5.9 to 6.5 GHz, as well as evidence at other frequencies.

CISR spectral plots for spectrometer channels 1 to 8 in Figure 16 show a large number of wideband sources, at frequencies of 5970, 6025, 6080, 6120, 6190, 6225, and 6250 MHz. Narrowband sources at 5530, 5591, 5608, and 5725 MHz among others are observed. The extremely high brightnesses in PSR main channel 1 appear correlated to the majority of the wideband sources, including the 5970, 6025, and 6190 MHz emitters. The narrowband sources in most cases contribute lower level RFI, for example IDAT analysis shows the 5591 MHz source in the right hand portion of the main channel 1 image at times near 17:14:55. The 6190 and 6250 MHz wideband sources also appear to contribute to the large image response in PSR main channel 2 observed around times 17:14 to 17:16.

CISR measurements of spectrometer channels 9 to 16 (Figure 17) continue to show the presence of strong wideband sources, particularly in channel 9 where sources at 6320 and 6370 MHz are observed. The increased power observed in Figure 17 for samples between 50 to 60 appears correlated to the general increase in all PSR channels near time 17:19, and is likely not caused by a specific source. Narrowband sources near 6555, 6580, 6622, 6631, 6770, 6791, 6808, 6861, and 6905 MHz are also observed, among others, and contribute to a lower-level corruption of the measurement that will be examined in detail in the future. The narrowband sources above 6600 MHz are also observed in PSR main channel 3 image, and correlate well with the brighter portions of the image.

Results for channels 17 to 22 in Figure 18 show a reduced level of RFI in these channels, although sources are still observable, for example near 7323 MHz. This source correlates well with increased brightnesses in the PSR main channel 4 image, although the color scale used in that image is not fine enough to show these small contributions.

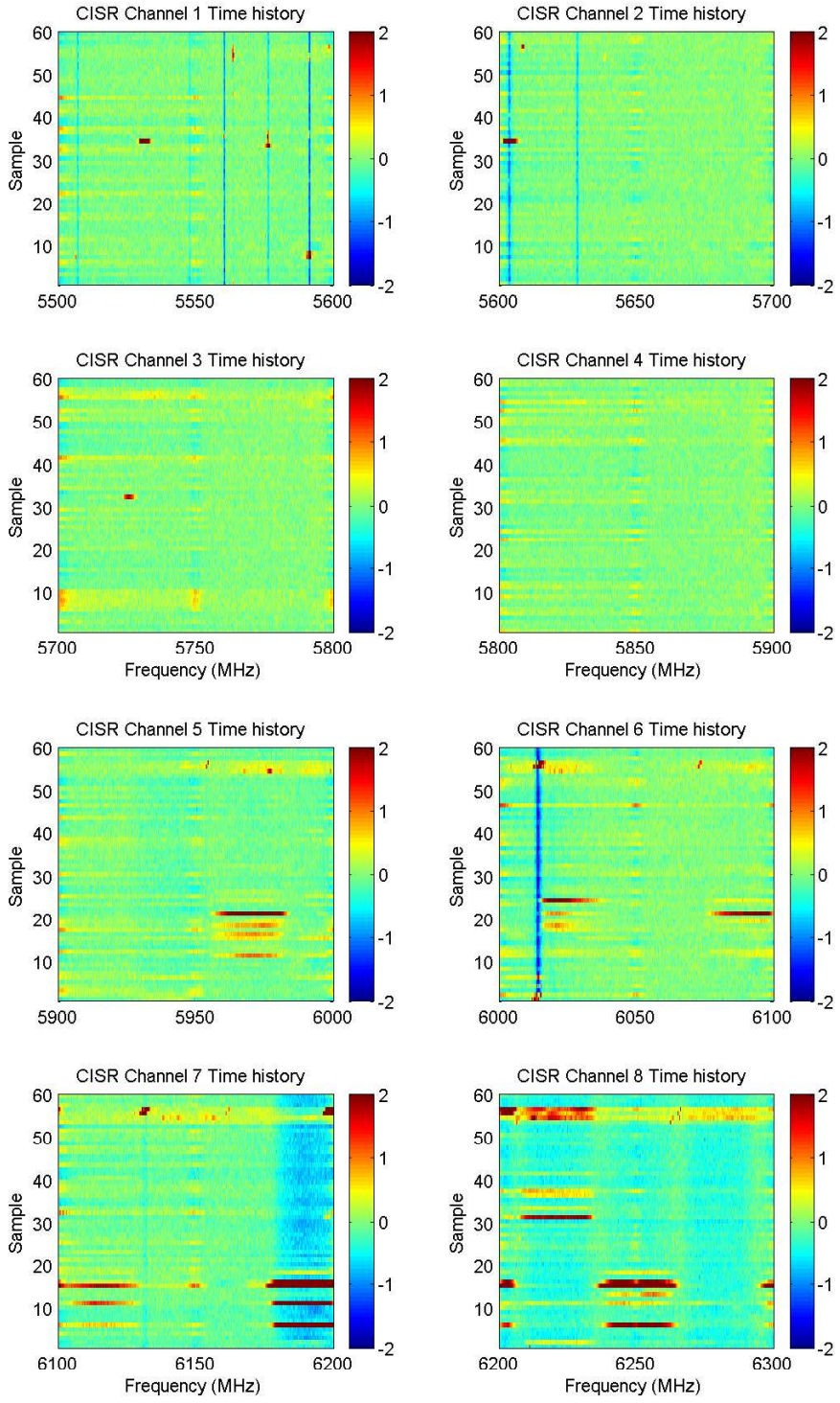

Figure 16: Same as Figure 6

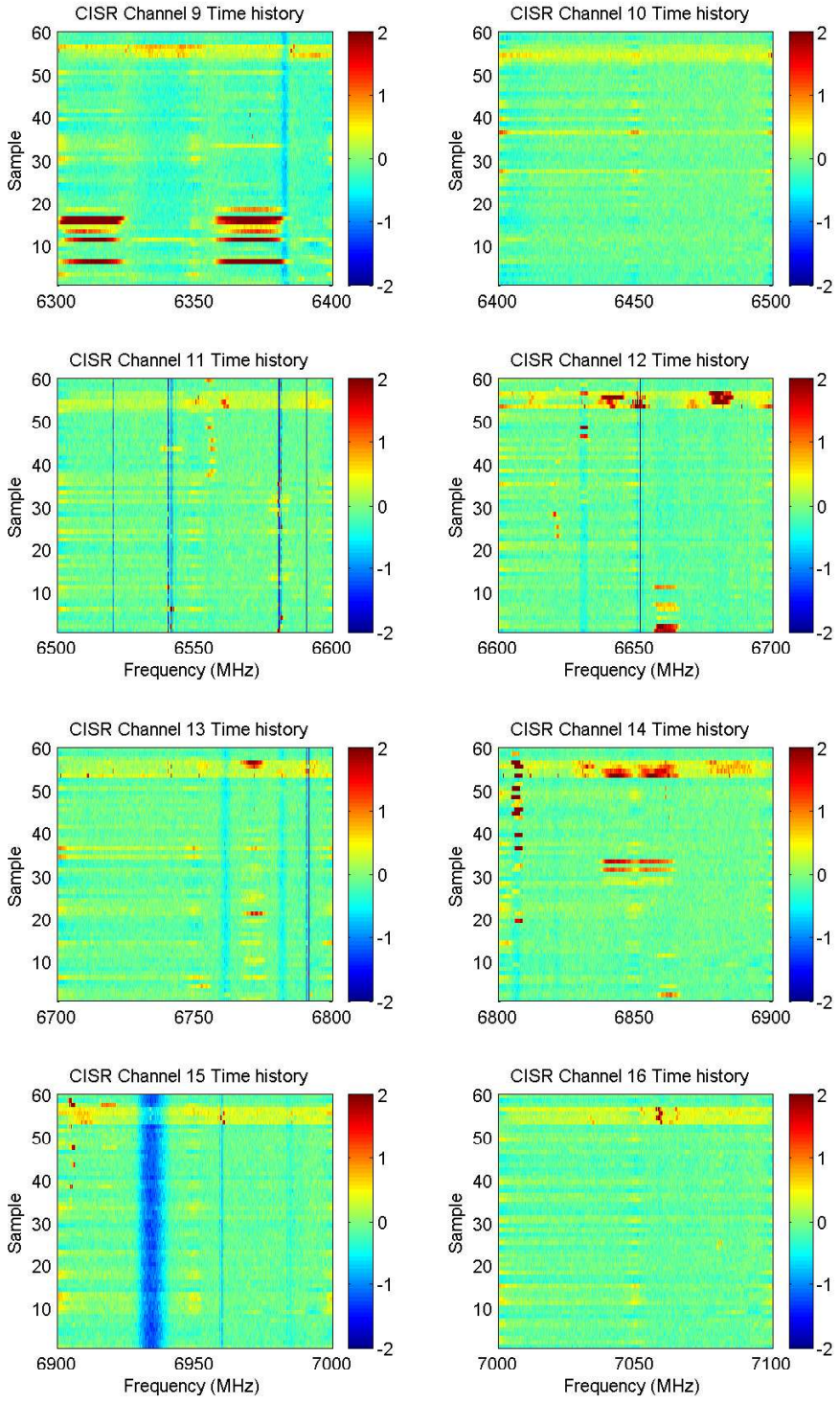

Figure 17: Same as Figure 7

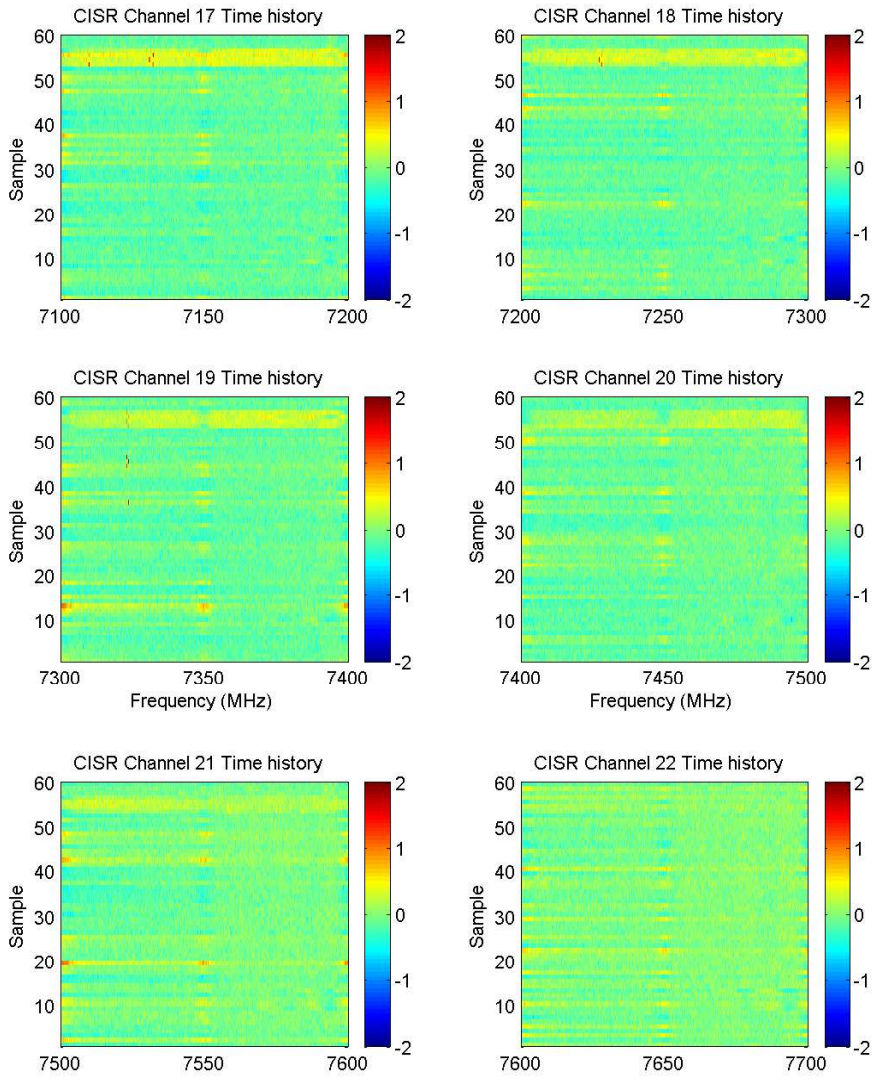

Figure 18: Same as Figure 8

7 Stare Mode During Transit back to WFF

The "stare mode" data obtained during transit from the at-sea measurements back to WFF offer interesting possibilities for analysis. These data are advantageous in that no scanning of the antenna is performed, so that a sweep of spectrometer channels can observe similar geographical locations if the aircraft velocity is moderate. Here an initial report on these data is provided, but further analysis will be performed to combine spectrometer channels into a geographic map once the navigational data is available.

Although the stare mode data is not entirely appropriate for an imaging process, Figure 19 illustrates the PSR main channel data in an image form, where the cross dimension is simply a means for extending the length dimension. Here time is progressing first from left to right in the image and then from lower to upper. Comparison of the data in the four channels again shows evidence of RFI, particularly in channels 1 and 3, where bright lines are observed that are absent in the other channels. The scene apparently includes primarily over-water observations with possible overflight of an small land feature near time 17:57 before return to water before landing.

Spectrometer channel time histories in Figure 20 show evidence of RFI at varying locations. The PSR linear channel in particular shows strong responses around 5.7-6. GHz and 6.2-6.5 GHz. Overflight of the land feature is apparent in all channels as well.

CISR spectra for channels 1 to 8 in Figure 21 show primarily narrowband sources, with the exception of a strong wideband source encountered near landing at 6190 MHz; this source has been encountered in all datasets examined. Narrowband sources at 5515, 5576, 6015, 6102, 6152, and 6208 MHz are observed, among others. The sources at 5515 and 5576 MHz appear correlated to the PSR main channel 1 response near time 17:53:59, although it is unlikely that these near out-of-band sources would produce the entire response observed in the image. Sources at 5615, 5778, 6015, and 6152 MHz appear in the land overflight portion of the PSR main channel 1 image, but apparently contribute lower levels of RFI. Other narrowband sources are observed

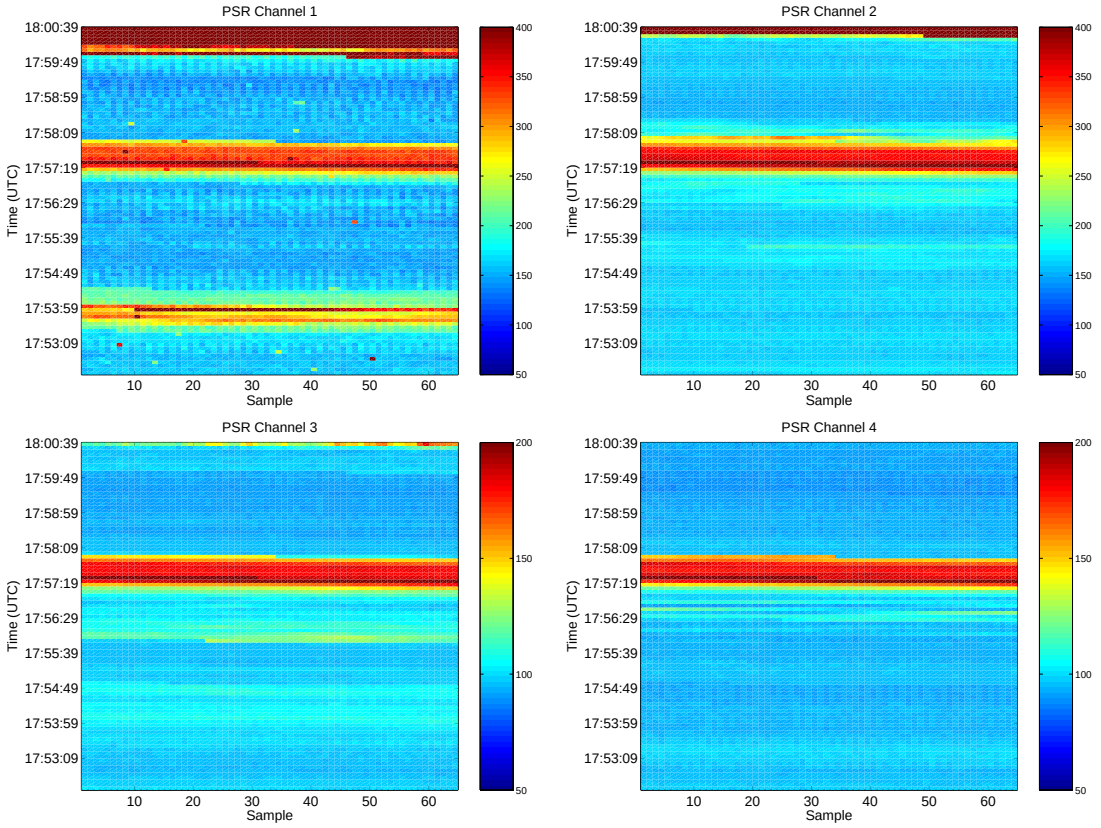

Figure 19: Calibrated brightnesses observed in 4 PSR main channels for stare mode operations on transit back to WFF

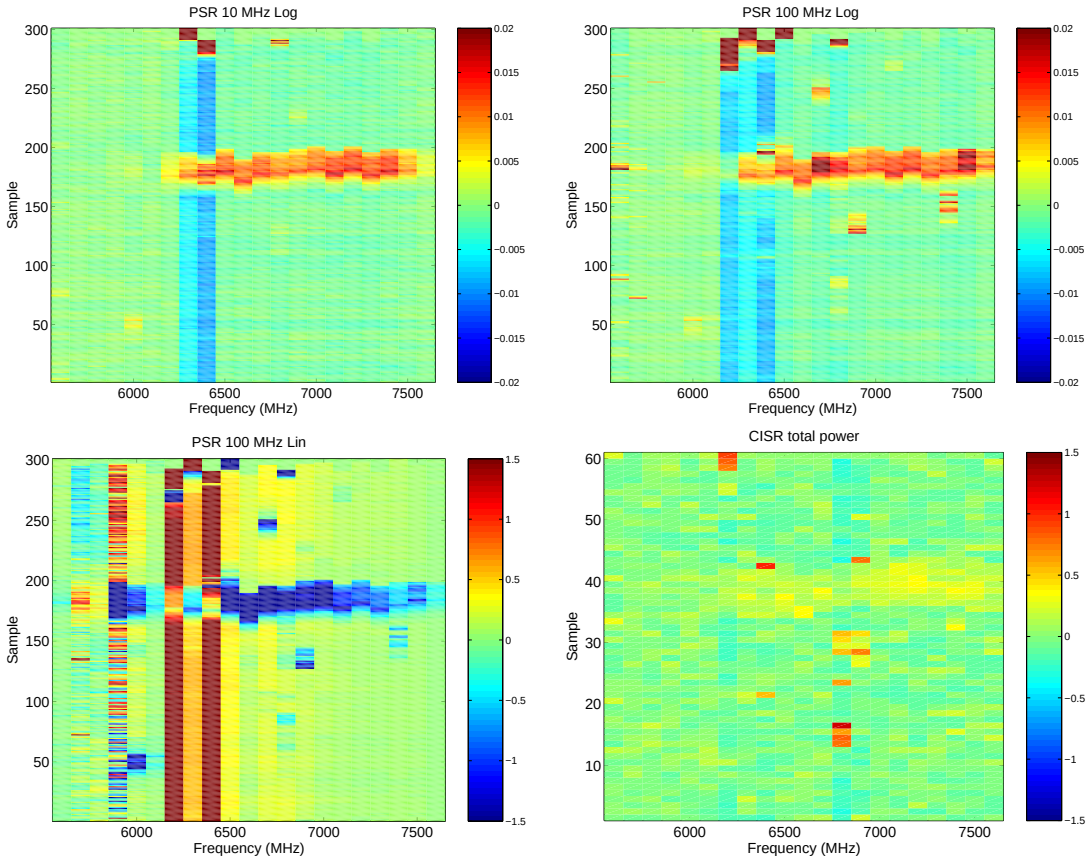

Figure 20: Same as Figure 5

in portions of the image over water from 17:54-17:57. These will be good additional good candidates for examination of low-level RFI effects.

Spectrometer channels 9 to 16 again show numerous narrowband sources in the CISR measurements, along with a somewhat wideband source near 6770 MHz. Source frequencies of 6326, 6386, 6560,6612, 6630, 6688, 6790, 6862, 6964, and 7035 MHz are observed among others. These sources are all observed in over water portions of the images in PSR main channels 2 and 3, with the exception of the 6688 MHz source, which appears near the land overflight at 17:57. Again these sources are excellent candidates for studying low-level RFI.

Finally, CISR measurements of spectrometer channels 17 to 22 in Figure 23 are dominated by a wideband interferer at 7325 MHz, located in the main channel four image at approximately 17:56. Other narrowband interferers at 7109, 7495, and 7505 MHz are also observed. The latter two sources may be a wideband source split across spectrometer channels 20 and 21.

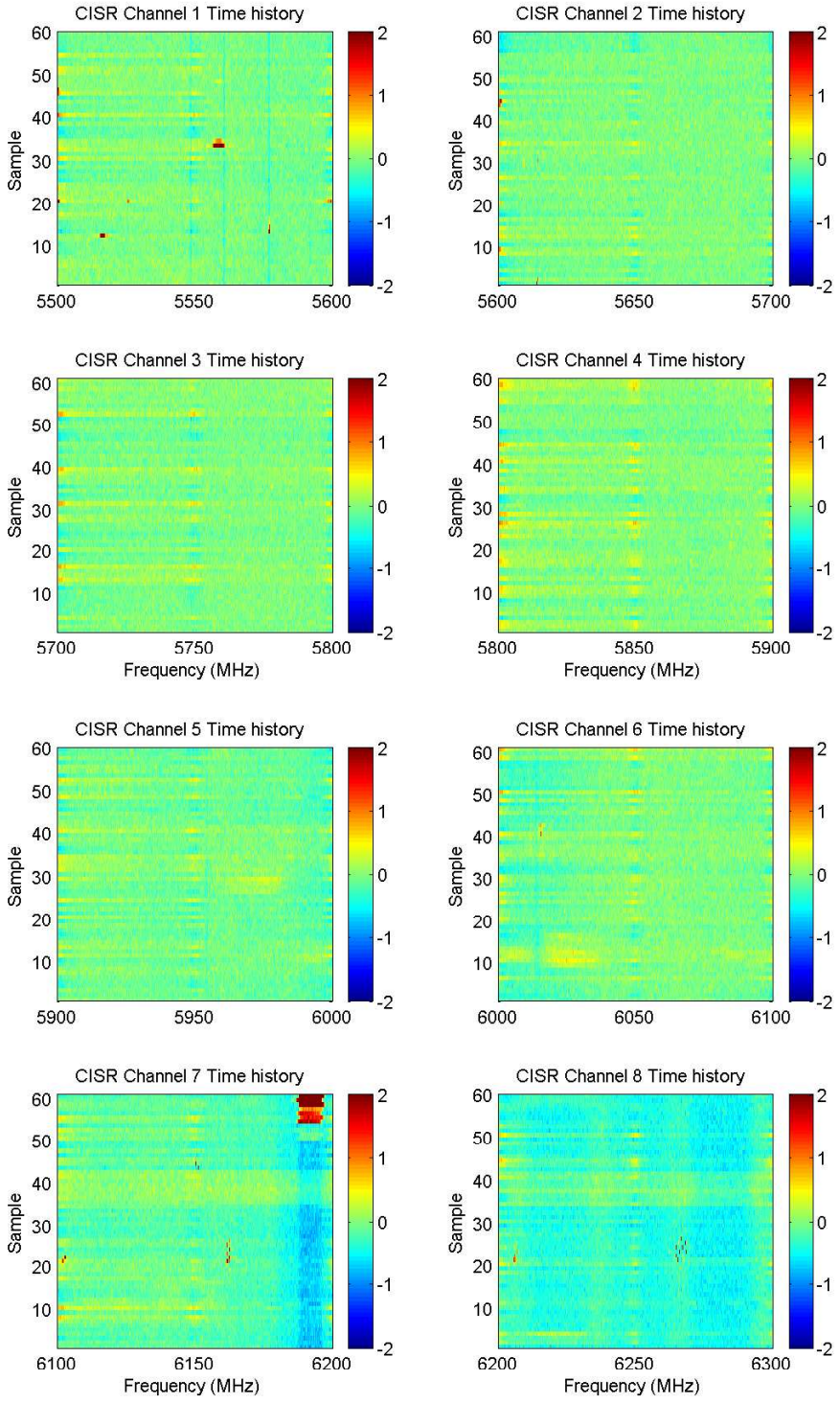

Figure 21: Same as Figure 6

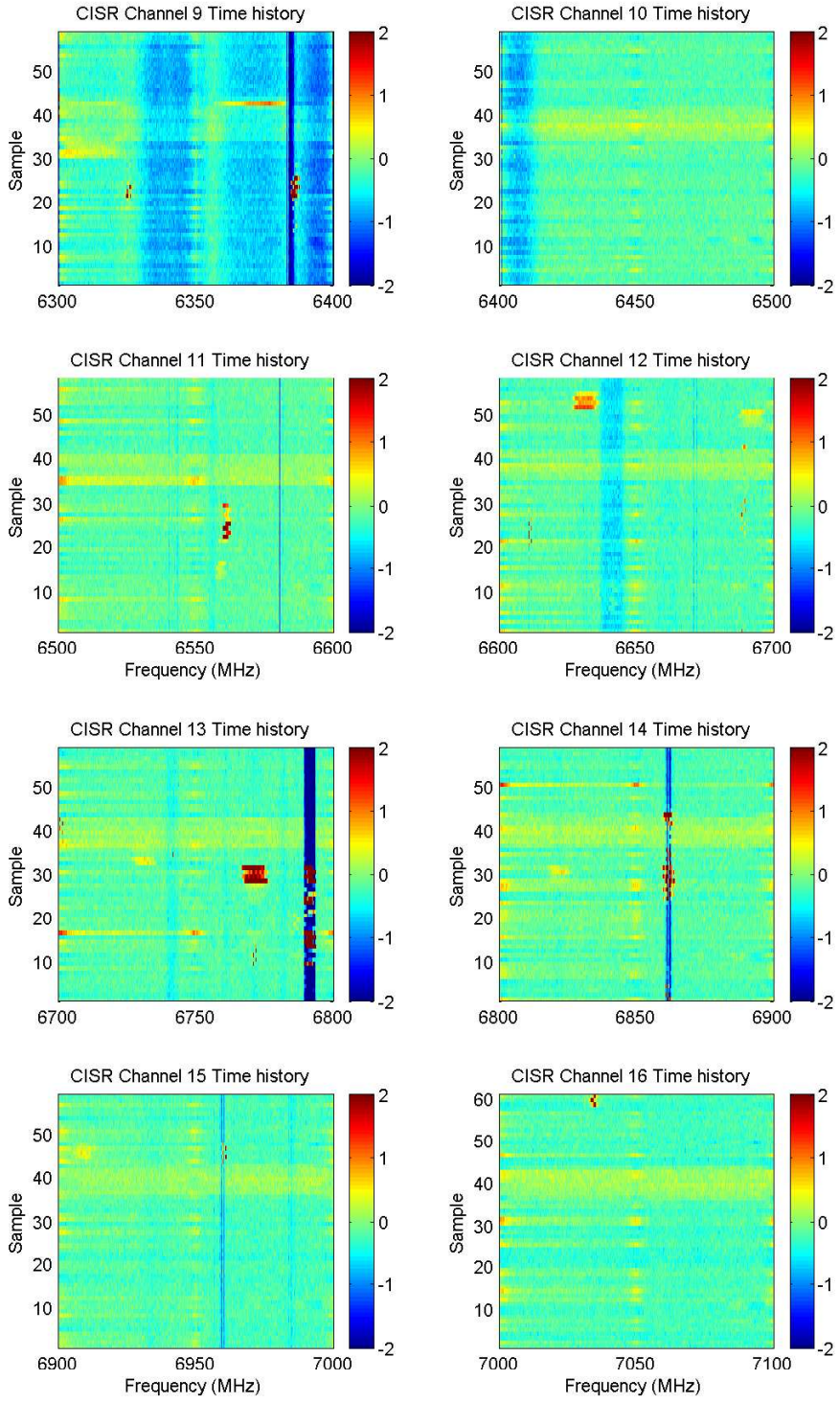

Figure 22: Same as Figure 7

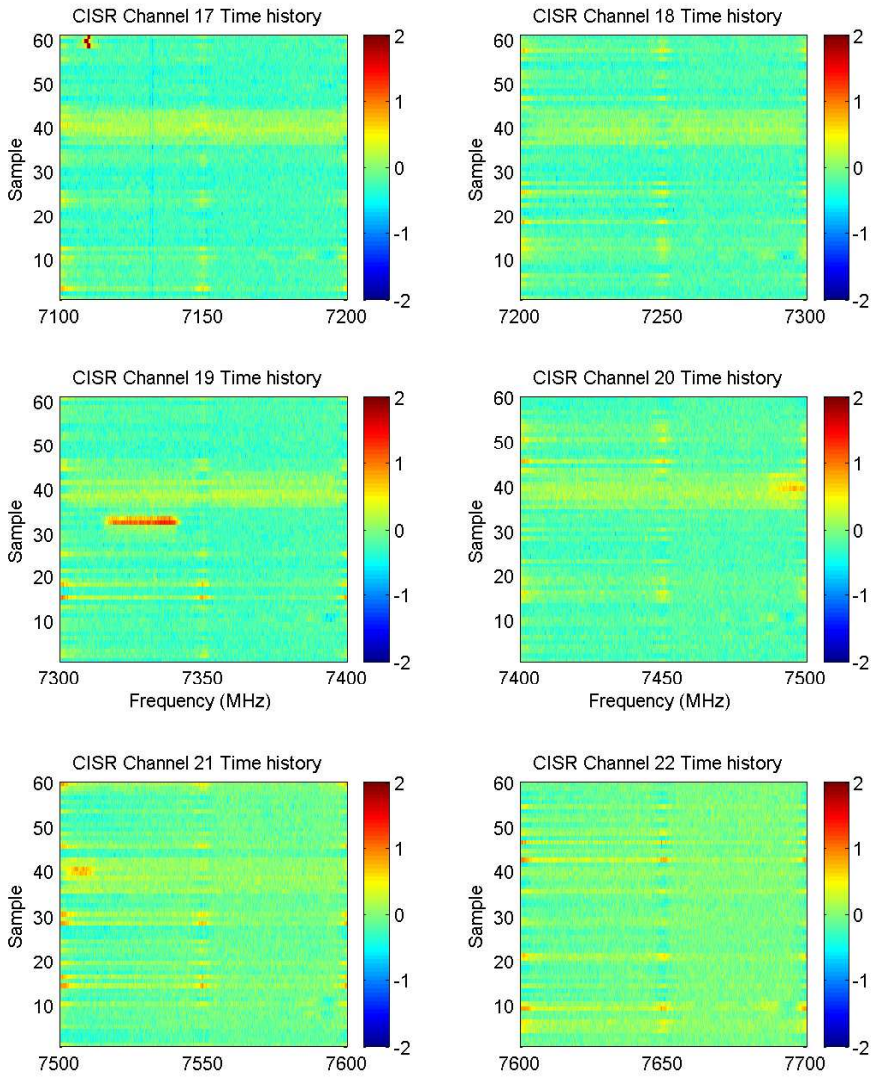

Figure 23: Same as Figure 8

8 Summary and Discussion

An initial examination of the dataset obtained from the October 8th PSR/CXI and CISR test flight has been provided. The 90 minutes of joint data contains observations of a variety of scenes, including strong and weak RFI environments. The data clearly show the possibility of significant corruption of measured brightnesses for wide channels throughout C-band, with the higher frequencies typically observing less but still appreciable corruption. Additional analyses are in progress to examine the effectiveness of various RFI suppression strategies on eliminating contributions from the sources observed. In particular, the performance of new mitigations made possible by CISR will be compared against the existing PSR 4 main channel suppression algorithm. Although it should be expected that the existing PSR algorithm will be successful in removing many cases of strong RFI, performance for weak RFI remains an issue. The higher temporal and spectral resolution available from CISR should enable removal of weak RFI beyond that of the existing algorithm. Further studies are also planned to classify spectral and temporal properties of the observed RFI sources. The addition of the navigational data should also enable a co-location of sources with any existing databases of emitters at C-band. Finally, data from the PSR/CXI vertically polarized and polarimetric channels (channel 3 only) at C band will be investigated, as well as an initial investigation of RFI observed in the PSR/CXI X-band channels.

Unfortunately, CISR experienced a hard drive failure following the test flight, and was unable to acquire data for the remainder of the AASI campaign. However since much of this campaign was over polar regions, and the transit flights were primarily over sea, the utility of CISR data in this campaign for RFI studies was not guaranteed. It is recommended that continued flights of the joint PSR/CXI system be considered so that RFI observations in a larger variety of RFI environments can be obtained.

References

[1] J. T. Johnson, A. J. Gasiewski, G. A. Hampson, S. W. Ellingson, R. Krishnamarachi, and M. Klein, "Airborne radio frequency interference studies at C-band using a digital receiver," *Int'l Geoscience and Remote Sensing Symposium (IGARSS 04),* conference proceedings, 2004.

[2] Gasiewski, A. J., M. Klein, A. Yevgrafov, and V. Leuski, "Interference mitigation in passive microwave radiometry," *Int'l Geoscience and Remote Sensing Symposium (IGARSS 02),* conference proceedings, 2002.

[3] MicroLambda Website, http : //www.microlambdawireless.com /YIG − Oscillators/EMYTOs/X − Series − SatCom.htm .

[4] J. T. Johnson and S.W. Ellingson, "Digital Receiver with Interference Suppression for Microwave Radiometry," 2001. http://esl.eng.ohio-state.edu/∼swe/iip/docserv.html.